DOI: 10.1002/cphc.201000350

Transverse Relaxation of Scalar-Coupled Protons

Takuya F. Segawa,[a] Bikash Baishya,*[a] and Geoffrey Bodenhausen[a, b]

In a preliminary communication (B. Baishya, T. F. Segawa, G. Bodenhausen, *J. Am. Chem. Soc.* **2009**, *131*, 17538–17539), we recently demonstrated that it is possible to obtain clean echo decays of protons in biomolecules despite the presence of homonuclear scalar couplings. These unmodulated decays allow one to determine apparent transverse relaxation rates R_2^{app} of individual protons. Herein, we report the observation of R_2^{app} for three methyl protons, four amide H^N protons, and all 11 backbone H^α protons in cyclosporin A. If the proton resonances overlap, their R_2^{app} rates can be measured by transferring their magnetization to neighboring ^{13}C nuclei, which are less prone to overlap. The R_2^{app} rates of protons attached to ^{13}C are faster than those attached to ^{12}C because of ^{13}C–^{1}H dipolar interactions. The differences of these rates allow the determination of local correlation functions. Backbone H^N and H^α protons that have fast decay rates R_2^{app} also feature fast longitudinal relaxation rates R_1 and intense NOESY cross peaks that are typical of crowded environments. Variations of R_2^{app} rates of backbone H^α protons in similar amino acids reflect differences in local environments.

1. Introduction

Spin-echo experiments[1–3] are widely used to measure homogeneous transverse relaxation rates whenever the decay of magnetization is partly determined by inhomogeneous broadening.[4] Spin-echo experiments are also used to evaluate translational diffusion coefficients[5,6] and electrophoretic mobility,[7] and to separate linewidth contributions arising from chemical exchange and homogeneous transverse relaxation.[8–17] Echo modulations due to homonuclear scalar couplings may render the determination of transverse relaxation rates of individual spins difficult, in particular when ^{13}C or ^{15}N nuclei are isotopically enriched, and of course for protons, which usually feature extensive networks of scalar couplings. To avoid echo modulations, most studies have so far been restricted to isolated or selectively labeled ^{13}C or ^{15}N spins. Recently, we demonstrated how to measure "apparent" transverse relaxation rates of backbone and side-chain protons in cyclosporin A (CsA) under conditions where the echo modulations that normally arise from homonuclear scalar couplings (^mJ with $m \geq 2$) are largely "quenched".[18] In Carr–Purcell–Meiboom–Gill (CPMG) multiple refocusing sequences $(\pi/2)_y-[\tau-\pi_x-\tau]_{2n}$ with pulse repetition rates $\nu_{rep}=1/(2\tau+\tau_\pi)$ and radio-frequency (rf) fields of intermediate strength (see below), echo modulations will vanish provided that one avoids harmonic relationships between the offsets and pulse repetition rates. In particular, echo modulations are quenched if the rf carrier is set on-resonance for a spin I of interest (offset $\Omega_I=0$), provided one avoids any coincidence between the offset Ω_S of the coupling partner S with multiples of the pulse repetition rate, that is, provided $\Omega_S \neq 2k\pi\nu_{rep}$, where k is an integer. In other words, modulations can be quenched by choosing a pulse repetition rate ν_{rep} that does not coincide with any subharmonic of the difference in chemical shifts $(\Omega_S-\Omega_I)$, that is, if $\nu_{rep} \neq \Omega_S/(2k\pi)$ when $\Omega_I=0$.[19] The quenching results from cumulative effects of nonideal pulses with "tilted" effective fields. This tilt is expressed by the parameter $\gamma_S=\Omega_S/\omega_1$, where ω_1 is the rf amplitude.

Herein, we explore three side-chain methyl CH_3 protons, four amide H^N protons, and all 11 backbone H^α protons in CsA. Backbone protons with fast R_2^{app} rates also feature fast longitudinal relaxation rates R_1. These protons also have intense NOESY cross peaks characteristic of crowded environments.

For fast pulse repetition rates, that is, if $\nu_{rep} > \Omega_S/(2\pi)$, the offsets are averaged out, hence R_2^{eff}, as defined by Tosner et al.,[20] is identical to the true transverse relaxation rate R_2. In this case, R_2^{app} as defined in our work[18,21] will also be identical to R_2, except if the chemical shift anisotropy (CSA) or external random field contributions are different for the two spins. For slow pulse repetition rates, that is, if $\nu_{rep} < \Omega_S/(2\pi)$, the two spins I and S can have different relaxation rates R_2^{app}. For very slow pulse repetition rates $\nu_{rep} < J_{IS}$, a partial conversion of in-phase into antiphase coherence (e.g., $I_x \rightarrow 2I_yS_z$) during the τ delays may affect the average relaxation rates R_2^{app}, bearing in mind that I_x and $2I_yS_z$ can have different decay rates.[22] We observed empirical correlations between R_2^{app}, R_1, and the intensities of NOESY cross peaks. These correlations are more pronounced when similar protons are compared between similar amino acid residues, for example, when comparing H^α protons

[a] T. F. Segawa, Dr. B. Baishya, Prof. Dr. G. Bodenhausen
Laboratoire de Résonance Magnétique Biomoléculaire
Institut des Sciences et Ingénierie Chimiques
Ecole Polytechnique Fédérale de Lausanne
BCH, 1015 Lausanne (Switzerland)
Fax: (+41) 21-6939435
E-mail: bikash.baishya@epfl.ch

[b] Prof. Dr. G. Bodenhausen
Département de Chimie, associé au CNRS
Ecole Normale Supérieure
24 rue Lhomond, 75231 Paris Cedex 05 (France)

in the four Me-Leu residues or H^{α} protons in the two Ala residues. This supports the view that, although the experimental transverse relaxation rates have prudently been called "apparent" so far, they do provide insight into the underlying relaxation mechanisms. If the proton resonances overlap, we can transfer the proton magnetization to directly bound ^{13}C spins (which are usually well resolved in the ^{13}C spectrum) by inserting a sequence for refocused insensitive nuclei enhanced by polarization transfer (INEPT) at the top of the 2*n*th echo. This procedure allows us to compare the monoexponential decays of protons attached to ^{12}C (by direct ^{1}H detection) with those of the same protons attached to ^{13}C (by using indirect detection).

It should be mentioned that *selective* refocusing pulses with $\omega_1 \ll \Omega_S$ do not offer an attractive alternative to quench scalar couplings between protons, for such pulses would have to be quite long, so that relaxation and evolution under scalar couplings during the pulses would have to be taken into account.

2. Results and Discussion

For systems with scalar-coupled protons in peptides and proteins, quenching of echo modulations in multiple refocusing sequences with nonideal pulses can be quite effective.

2.1. Effect of Offsets on Echo Modulations

When the spin *I* under investigation is on-resonance ($\Omega_I = 0$), echo modulations due to homonuclear scalar couplings, such as $^{3}J(H^{\alpha}H^{\beta})$, $^{3}J(H^{\alpha}H^{N})$ between protons or $^{1}J(C^{\alpha}C^{\beta})$, $^{1}J(C^{\alpha}C')$ between carbon nuclei, are most pronounced at pulse intervals τ that satisfy the following "recoupling conditions" [Eq. (1)]:[21]

$$\tau = (k\pi/\Omega_S - \pi/4\,\omega_1) \qquad (1)$$

This equation implies that for a given rf amplitude ω_1 the echoes will remain unmodulated for most durations τ provided the offset term Ω_S is small, that is, when the intervals between the recoupling conditions $\Delta\tau = \pi/\Omega_S$ are large. In other words, recoupling effects will appear only after long τ intervals. Figure 1 A shows simulations (neglecting relaxation) of the modulation of single-quantum coherence (SQC) I_x as a function of the interval τ for even-numbered echoes. For comparison, we show the effect of the offset Ω_S keeping the same ratio $\gamma = \Omega_S/\omega_1$ and keeping the same scalar coupling constant $J_{IS} =$ 8.4 Hz. The coherence I_x is monitored at the top of the 30th echo excited with the sequence $[\tau - \pi_x - \tau]_{2n}$ with $n = 15$. In Figure 1 A, the blue line corresponds to offsets $\Omega_I = 0$ and $\Omega_S/(2\pi) = 1.40$ kHz, with an rf amplitude $\omega_1/(2\pi) = 5.05$ kHz, so that $\gamma = \Omega_S/\omega_1 = 0.28$. The red line describes $\Omega_I = 0$ and $\Omega_S/(2\pi) = 4.317$ kHz, with $\omega_1/(2\pi) = 15.54$ kHz, hence we have again the ratio $\gamma = \Omega_S/\omega_1 = 0.28$. We can see that large offsets (e.g., the red line) lead to recoupling conditions that appear closely spaced in the time domain.

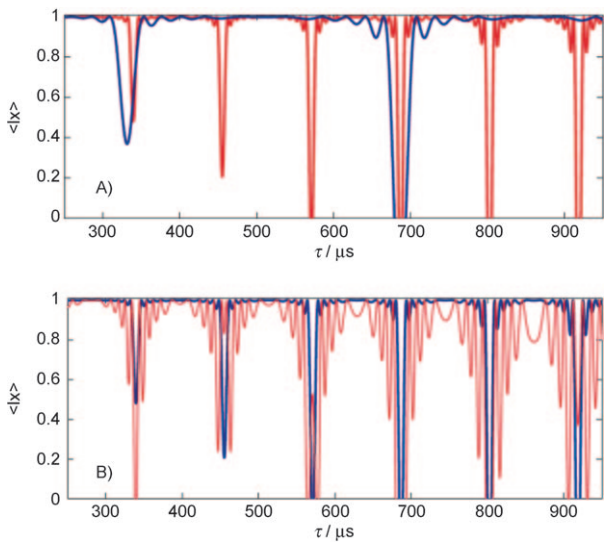

Figure 1. Simulations (without considering relaxation) of the modulations of the 30th echo ($n = 15$) of in-phase coherence I_x in a homonuclear two-spin system *I*–*S* as a function of the interval τ in the echo sequence $[\tau - \pi_x - \tau]_{2n}$. A) For a ratio $\gamma = \Omega_S/\omega_1 = 0.28$ and a given coupling constant $J = 8.4$ Hz, the effect of the offset of the coupling partner is illustrated for $\Omega_S/(2\pi) = 4.31$ (red line) and 1.406 kHz (blue line). B) For a ratio $\gamma = \Omega_S/\omega_1 = 0.28$ and a given offset $\Omega_S/(2\pi) = 4.31$ kHz, the effect of the scalar coupling is shown for $J = 35$ (red line) and $J = 8.4$ Hz (blue line).

2.2. Effect of Scalar Couplings on Echo Modulations

Figure 1 B shows simulations of modulations of a coherence I_x observed at the top of the 30th echo ($n = 15$), as a function of the scalar coupling constant for a given ratio $\gamma = 0.27$ and a fixed offset $\Omega_S/(2\pi) = 4.31$ kHz. The blue line shows the effect of $J_{IS} = 8.4$ Hz, while the red line shows modulations due to $J_{IS} = 35$ Hz. It can be seen that small couplings can be averaged out more effectively than large couplings. The red line shows strong modulations even in regions between two adjacent recoupling conditions, whereas the modulations are negligible for the blue line. Thus, the simulations predict that quenching will be more effective in spin systems with reasonably small offsets (though they should not be so small that strong coupling effects take their toll) and small scalar coupling constants. Protons in proteins and peptides often fulfill these conditions. The scalar couplings $^{3}J(H^{\alpha}H^{\beta})$ or $^{3}J(H^{\alpha}H^{N})$ often fall in the range between 5 and 11 Hz, much smaller than $^{1}J(C^{\alpha}C^{\beta})$ and $^{1}J(C^{\alpha}C')$, which lie in the range between 35 and 55 Hz.[23] In addition, typical offsets between H^{α} and H^{β}, or between H^{α} and H^{N}, are much smaller than those between C^{α} and C^{β} or C^{α} and C'.

2.3. Apparent Relaxation Rates R_2^{app} Determined by Direct Proton Detection

To investigate R_2^{app} of scalar-coupled protons experimentally, we considered the cyclic undecapeptide CsA. The NMR spectrum has been assigned by Oschkinat et al.[24,25] The chemical structure and the numbering of the amino acids are shown in Figure 2 A. A TLC-grade sample was obtained from Sigma–Al-

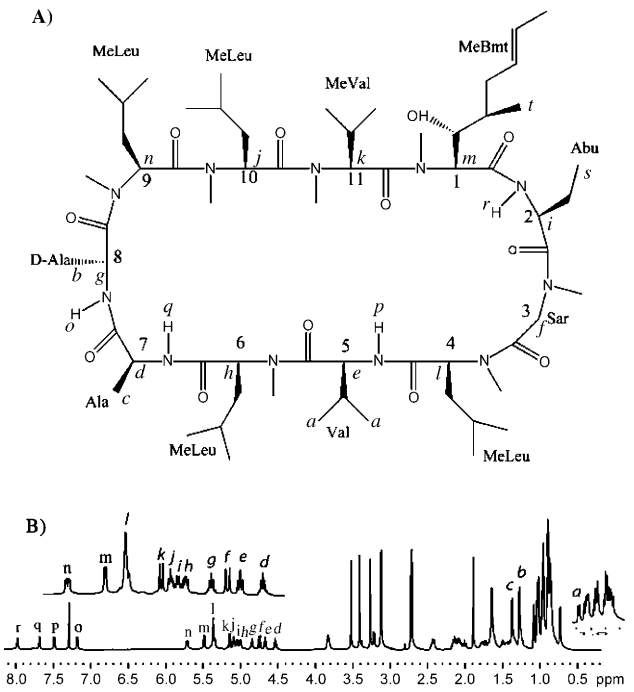

Figure 2. A) Structure of CsA with its amino acids numbered 1 to 11. The apparent transverse proton relaxation could be determined for a few selected protons labeled "*a*" to "*r*". B) Proton spectrum of CsA in $CDCl_3$ at 500 MHz and 300 K. The three methyl doublets labeled "*a–c*" at 1.08, 1.27, and 1.37 ppm stem from Val5, D-Ala8, and Ala7, respectively; the 11 H^{α} multiplets labeled "*d–n*" at 4.53, 4.67, 4.74, 4.84, 4.99, 5.04, 5.08, 5.15, 5.35, 5.47, and 5.72 ppm are due to Ala7, Val5, Sar3, D-Ala8, MeLeu6, Abu2, MeLeu10, MeVal11, MeLeu4, MeBmt1, and MeLeu9, respectively; and the four amide H^N signals labeled "*o–r*" at 7.18, 7.48, 7.68, and 7.98 ppm are identified with D-Ala8, Val5, Ala7, and Abu2, respectively.

drich and dissolved in $CDCl_3$. The proton spectrum in Figure 2B shows many well-resolved multiplets in the H^N (*o–r*) and H^{α} (*d–n*) regions, and a few nonoverlapping methyl peaks (*a–c*). Note that the signals have been relabeled with respect to our earlier work.[18] In order to choose appropriate rf amplitudes and repetition rates, the offsets of the coupling partners were determined from a COSY spectrum. The integrals of 18 selected multiplets were recorded using the so-called "hybrid" approach.[26] In this manner, favorable quenching conditions can easily be identified empirically without resorting to theory or simulations. Figure 3 shows echo amplitudes recorded with the hybrid sequence $[\tau-\pi_x-\tau]_{2n}$ as a function of τ at the top of the 2*n*th echo for the H^N and methyl protons, while Figure 4 shows the H^{α} protons.

The peaks marked "*a*" to "*r*" in Figure 2B were investigated by recording unmodulated echo decays, after choosing favorable τ delays (highlighted in Figures 3 and 4) and incrementing *n*. The smallest (and therefore most critical) offset investigated was for the methyl protons H^{γ} in Val5 of multiplet *a*, where the offset to the neighboring H^{β} protons was only 710 Hz while $^3J(H^{\beta}H^{\gamma})=6.55$ Hz and the rf amplitude was 5.6 kHz (ratio $\gamma=\Omega_S/\omega_1=0.12$). The R_2^{app} rates were determined by exponential fitting.

By way of example, consider the doublet of the proton $I=H^{\alpha}$ of MeVal11 (signal "*k*" in Figure 2B). The rf carrier was positioned at 5.15 ppm to be resonant with this H^{α} proton. Since there is only one resolved coupling $^3J(H^{\alpha}H^{\beta})=10.9$ Hz, the system can be treated as a two-spin system, provided one limits the observation to the H^{α} region. The offset of the coupling partner H^{β} is $\Omega_S/(2\pi)=1.5$ kHz. The ^4J couplings to the six protons of the two $C^{\gamma}H_3$ groups and the three protons of the NCH_3 group are not resolved. Figure 5A displays the amplitude of the integral of the multiplet obtained by Fourier transformation of the 60th echo ($n=30$) as a function of τ, that is, using the hybrid approach. For the 500th echo ($n=250$), the ^4J couplings to the nine remote protons give rise to three other weak "dips" for $\tau=430$, 677, and 705 µs (not shown).

Figure 5B shows monoexponential fits to the experimental decays of the H^{α} proton "*k*" recorded for increasing *n*, using favorable τ intervals chosen to avoid echo modulations (marked by a square, circle, and triangle in Figure 5A). All curves appear to be free of modulations and R_2^{app} can be determined by simple monoexponential fits. These rates are compared with experiments in which echo decays were monitored with a single refocusing π pulse of duration τ_{π} applied at $T/2=$

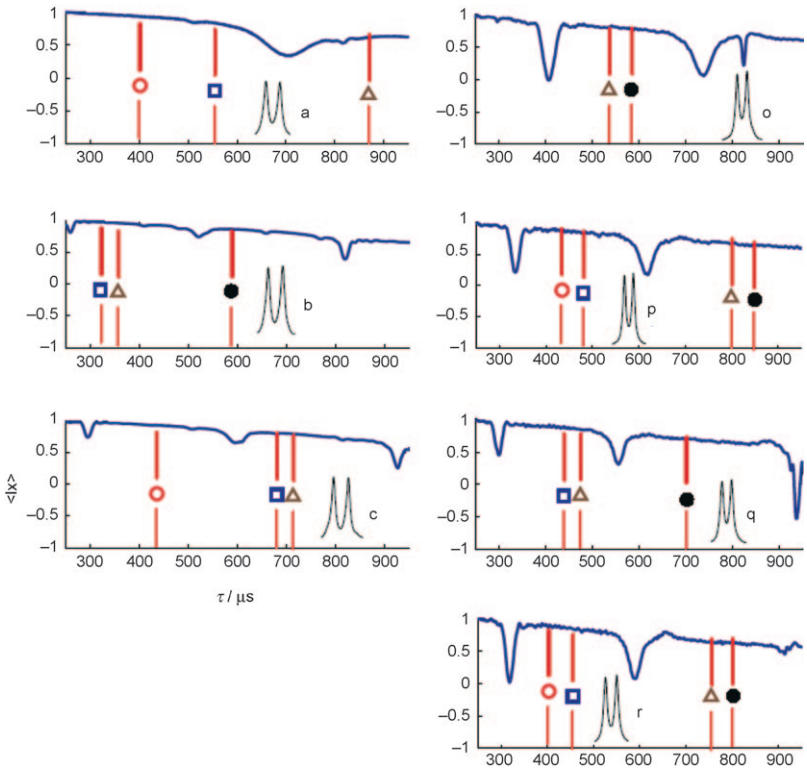

Figure 3. Amplitudes of the 60th echo ($n=30$) recorded by direct proton detection with hybrid sequences $(\pi/2)_y-[\tau-\pi_x-\tau]_{2n}$ as a function of τ for the protons "*a*" = Val5 CH^{γ}_3, "*b*" = D-Ala8 CH^{β}_3, "*c*" = Ala7 CH^{β}_3, "*o*" = D-Ala8 H^N, "*p*" = Val5 H^N, "*q*" = Ala7 H^N, and "*r*" = Abu2 H^N. The rf amplitude was 5.6 kHz in all cases. The offsets of the coupling partners, the magnitudes of the coupling constants, the ratios $\gamma=\Omega_S/\omega_1$, and the τ delays where echo modulations are most pronounced are listed in Table 1. The τ delays marked with □, ○, △ and ● are chosen for the measurements of R_2^{app} by incrementing *n* and reported in Table 1.

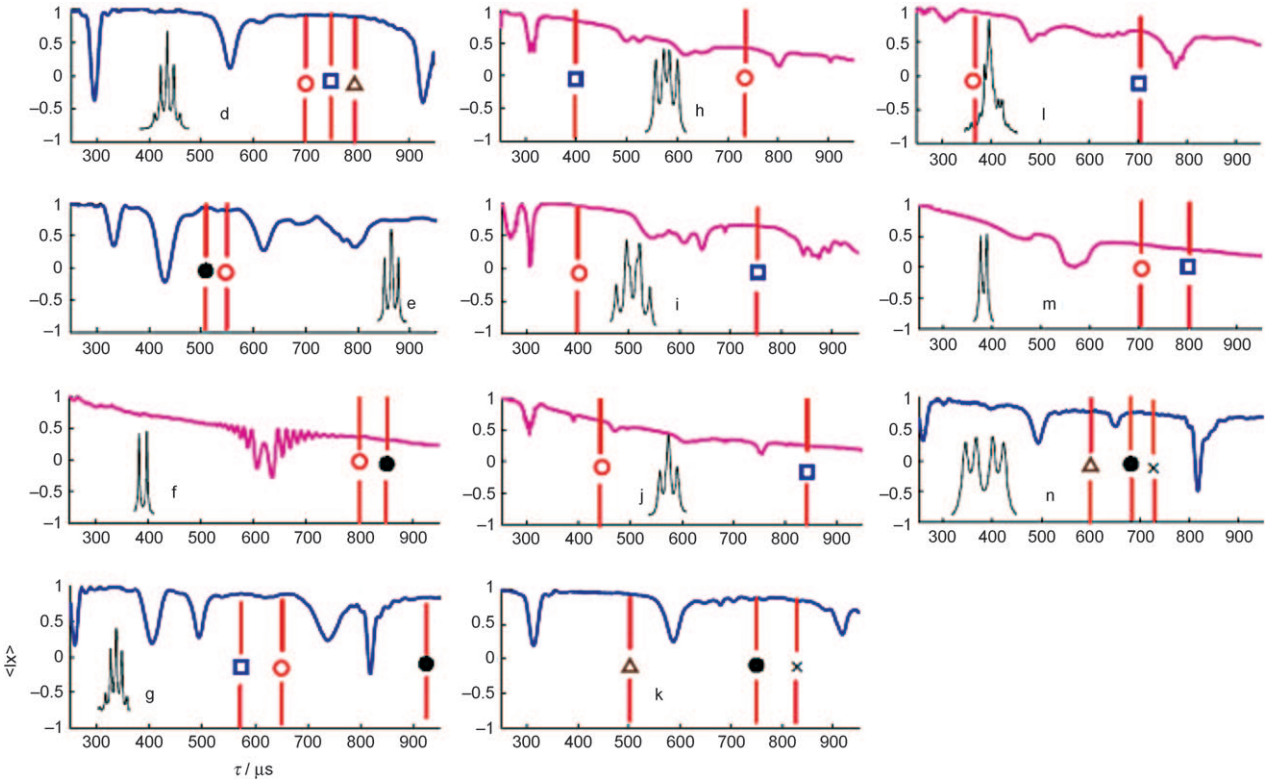

Figure 4. Signals of all 11 H^{α} protons in CsA recorded by direct detection using hybrid sequences. All curves were obtained by direct detection of H^{α} signals: "*d*" Ala7, "*e*" = Val5, "*f*" Sar3, "*g*" = D-Ala8, "*h*" = MeLeu6, "*i*" = Abu2, "*j*" = MeLeu10, "*k*" = MeVal11, "*l*" = MeLeu4, "*m*" = MeBmt1, and "*n*" = MeLeu9. The offsets of the coupling partners, the magnitudes of the coupling constants, the ratios $\gamma = \Omega_S/\omega_1$, and the τ delays where echo modulations are most pronounced are listed in Table 2. Blue curves: amplitudes of the 60th echoes ($n = 30$) of H^{α} protons recorded by direct detection with the hybrid sequence as a function of τ with an rf amplitude $\omega_1/(2\pi) = 5.6$ kHz. Red curves: amplitudes of the 320th echo ($n = 160$) recorded with $\omega_1/(2\pi) = 4$ kHz. The τ delays marked with □, ○, △ and ● are chosen for the measurements of R_2^{app} by incrementing n and reported in Table 1.

$n(2\tau+\tau_\pi)-\tau_\pi/2$ (Figure 5C). Fitting with a monoexponential decay multiplied by a cosine function (i.e., assuming a two-spin system) gives faster decay rates. It is difficult to define a fitting function that takes into account all unresolved ^4J couplings to the nine remote protons of the three methyl groups, since there may be several J couplings with different magnitudes. For larger biomolecules with faster relaxation rates and broader lines, fitting both R_2^{app} and J will be even more difficult. When the main coupling $^3J(H^{\alpha}H^{\beta})$ is quenched, long-range couplings have very weak effects. These can be quenched by using sequences with $750 < \tau < 850$ μs.

Figures 6 and 7 show monoexponential fits to unmodulated decays recorded with the sequence $[\tau-\pi_x-\tau]_{2n}$ for favorable τ intervals as a function of the number of cycles n for the H^N, H^{α} and methyl protons. Table 1 recapitulates the measured rates R_2^{app} and the experimental parameters utilized for protons "*a*–*c*" and "*o*–*r*", while Table 2 gives a summary of the 11 H^{α} protons from "*d*" to "*n*" along the backbone.

We compared the apparent transverse relaxation rates R_2^{app} with longitudinal relaxation rates R_1 determined by inversion recovery experiments, as shown in Tables 1 and 2. The intensities of NOESY cross peaks involving all 18 protons (attached to ^{12}C) and their neighbors were also investigated. The following trends are observed when similar protons in similar amino acids are compared:

1) For $R_1(H^{\alpha})$ in MeLeu residues, we observe the trend $R_1(H^{\alpha}$ in MeLeu4 "*l*") $= 1.2\ s^{-1} < R_1(H^{\alpha}$ in MeLeu6 "*h*") $= 2.36\ s^{-1} < R_1(H^{\alpha}$ in MeLeu10 "*j*") $= 3.02\ s^{-1} < R_1(H^{\alpha}$ in MeLeu9 "*n*") $= 3.08\ s^{-1}$. On the other hand, $R_2^{app}(H^{\alpha}$ in MeLeu4 "*l*") $= 1.74\ s^{-1}$ using $\nu_{rep} = 667$ Hz, $\Omega_S/(2\pi) = 1470$ and 1675 Hz, which is smaller than $R_2^{app}(H^{\alpha}$ in MeLeu6 "*h*") $= 3.03\ s^{-1}$ using $\nu_{rep} = 645$ Hz, $\Omega_S/(2\pi) = 1450$ and 1805 Hz, and yet smaller than $R_2^{app}(H^{\alpha}$ in MeLeu10 "*j*") $= 4.25\ s^{-1}$ using $\nu_{rep} = 565$ Hz, $\Omega_S/(2\pi) = 1495$ Hz and 1910 Hz and $R_2^{app}(H^{\alpha}$ in MeLeu9 "*n*") $= 4.37$ with $\nu_{rep} = 720$ Hz, $\Omega_S/(2\pi) = 1774$ and 2235 Hz. The strong NOESY cross peak observed between MeLeu10 ("*j*") and MeLeu9 ("*n*") is consistent with this evidence.
2) For H^{α} protons in Ala residues, we note that $R_2^{app}(H^{\alpha}$ in Ala7 "*d*") $= 1.22\ s^{-1}$ with $\nu_{rep} = 592$ Hz, $\Omega_S/(2\pi) = 1581$ and 1576 Hz is smaller than R_2^{app} (H^{α} in Ala8 "*g*") $= 1.75\ s^{-1}$ with $\nu_{rep} = 506$ Hz, $\Omega_S/(2\pi) = 1168$ and 1785 Hz. This trend is consistent with the longitudinal relaxation rates R_1("*d*") $= 0.95\ s^{-1} < R_1$ ("*g*") $= 1.31\ s^{-1}$. The H^{α} proton "*g*" of D-Ala8 is in a crowded environment, as can also be seen from the NOESY cross peak between H^{α} of D-Ala8 and the *N*-methyl protons of MeLeu9, while H^{α} in Ala7 is not involved in any NOESY cross peaks.[24]
3) For H^N in Ala residues, an opposite trend is observed, that is, Ala7 > D-Ala8, with $R_2^{app}(H^N$ in Ala7 "*q*") $= 6.53\ s^{-1}$,

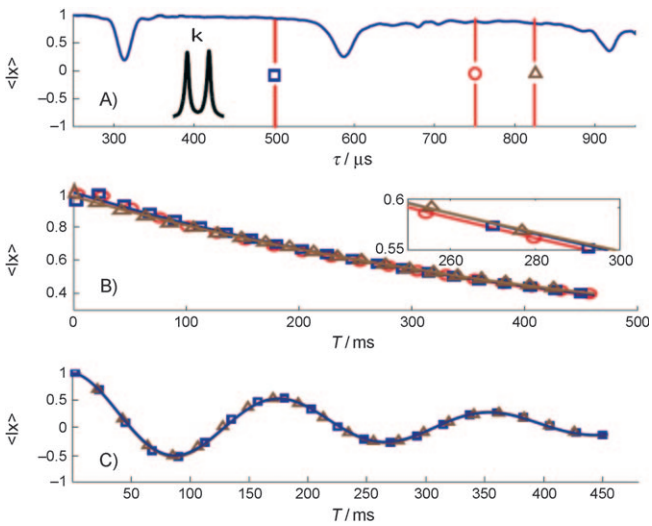

Figure 5. A) Amplitude of the H^{α} proton doublet "*k*" of MeVal11 in CsA recorded with the hybrid sequence $(\pi/2)_y-[\tau-\pi_x-\tau]_{2n}$ as a function of τ at the top of the 60th echo ($n=30$). The doublet arises from $^3J(H^{\alpha}H^{\beta})=10.9$ Hz. The rf carrier is positioned on resonance for the H^{α} proton "*k*" at 5.15 ppm. The offset of the coupling partner H^{β} is $\Omega_S/(2\pi)=1.5$ kHz. The rf amplitude of the refocusing pulses was $\omega_1/(2\pi)=5.6$ kHz (pulse length $\tau_{\pi}=89.2$ μs), that is, $\gamma=\Omega_S/\omega_1=0.27$. Three favorable intervals $\tau=500$, 750, and 825 μs where echo modulations can be neglected are marked with a square, an open circle, and a triangle, respectively. B) Decays of the H^{α} proton "*k*" recorded for these favorable τ intervals as a function of the number of cycles *n*. The unmodulated decays were fitted with monoexponential functions. For squares, open circles, and triangles with $\tau=500$, 750, and 825 μs, one finds $R_2^{app}=2.04$, 2.07, and 1.94 s^{-1}, respectively. For $\tau=500$ μs (squares), $n=1$, 10, 20, …, 200, so that the time axis $T=n(4\tau+2\tau_{\pi})$ extended over $0<T<450$ ms; for $\tau=750$ μs (open circles) $0<T<457.69$ ms; for $\tau=825$ μs (triangles) $0<T<426$ ms. C) Modulated decay of the H^{α} proton "*k*" obtained with a single refocusing π pulse applied at *T*/2. A fit with an exponential function multiplied by a cosine function gives $R_2^{app}=3.7$ s^{-1} and $J=10.9$ Hz.

using $\nu_{rep}=672$ Hz, $\Omega_S/(2\pi)=1578$ Hz $>R_2^{app}(H^N$ in Ala8 "*o*"$)=5.65$ s^{-1} using $\nu_{rep}=794$ Hz for $\Omega_S/(2\pi)=1170$ Hz. This is consistent with R_1("*q*")$=2.72$ $s^{-1}>R_1$("*o*")$=1.87$ s^{-1}. This time H^N in Ala7 features a NOESY cross peak with H^{α} of MeLeu6, while H^N in D-Ala8 is not involved in any NOESY cross peaks.

4) For H^{β} methyl protons in Ala residues, the trend Ala7 > D-Ala8 is observed, that is, $R_2^{app}(H^{\beta}$ in Ala7 "*c*"$)=3.7$ s^{-1} using $\nu_{rep}=593$ Hz for $\Omega_S/(2\pi)=1581$ Hz $>R_2^{app}(H^{\beta}$ in Ala8 "*b*"$)=3.2$ s^{-1} using $\nu_{rep}=680$ Hz for $\Omega_S/(2\pi)=1774$ Hz. This is consistent with R_1("*c*")$=2.53$ $s^{-1}>R_1$("*b*")$=2.36$ s^{-1}.

5) We also compared R_2^{app} and R_1 for all H^{α} protons along the backbone, irrespective of amino acid types. The following trends are observed:
R_1 (s^{-1})$=3.08$ ("*n*") > 3.02 ("*j*") > 2.89 ("*f*") > 2.36 ("*h*") > 2.15 ("*m*") > 1.54 ("*k*") > 1.42 ("*i*") = 1.42 ("*e*") > 1.31 ("*g*") > 1.20 ("*l*") > 0.95 ("*d*")
R_2^{app} (s^{-1})$=4.37$ ("*n*") > 4.25 ("*j*") > 3.74 ("*f*") > 3.02 ("*h*") < 3.60 ("*m*") > 2.02 ("*k*") > 1.72 ("*i*") < 2.00 ("*e*") > 1.75 ("*g*") > 1.74 ("*l*") > 1.22 ("*d*")

Except for two permutations of "*h*" with "*m*" and of "*i*" with "*e*", the rates R_2^{app} follow the same order as the R_1 values.

When we compare the rates R_2^{app} of similar protons in similar amino acids, protons with higher rates R_2^{app} appear to be closer to some other protons in neighboring amino acids. Of course, the local geometry is identical in a given amino acid, so that only neighboring amino acids can make a difference.

If the pulse repetition rates are higher than the offsets, the R_2^{eff} rates will be practically identical for both spins provided no external random field or CSA interaction are considered.[20] For example, H^{α} and H^N, or H^{α} and H^{β} in D-Ala8, feature almost the same R_2^{app}. An identical R_2^{app} does not allow one to distinguish stereochemically different local environments of the two spins. With slow pulse repetition rates, the averaging of the offset terms is slow and the two spins approach the limit of unlike spins with different relaxation rates, which may convey information about stereochemically different environments. This is indeed observed in our experiments. For example, in D-Ala8 the measured R_2^{app} values are very different for H^{α}, H^N, and H^{β} for nearly the same repetition rates and offsets: R_2^{app} (H^N in D-Ala8)$=5.65$ s^{-1} ($\nu_{rep}=794$ Hz, $\Omega_S/(2\pi)=1170$ Hz) > R_2^{app} (H^{β} in D-Ala8)$=3.3$ s^{-1} ($\nu_{rep}=788$ Hz, $\Omega_S/(2\pi)=1774$ Hz) > R_2^{app} (H^{α} in D-Ala8)$=1.75$ s^{-1} ($\nu_{rep}=801$ Hz, $\Omega_S4/(2\pi)=1170$, 1785 Hz).

In our experiments, the scalar coupling constants are in effect decoupled by cumulative pulse imperfections due to a large number of refocusing pulses. If the pulse repetition rates were very slow, that is, comparable to the magnitudes of typical homonuclear *J*-coupling constants, the evolution under the scalar couplings in the τ delays could partly convert in-phase terms I_x into antiphase terms $2I_yS_z$. The neighboring *S* spin could be interacting with more remote spins *R* through dipole–dipole interactions, or it could be subject to external random field effects, or indeed relax because of CSA. The relaxation rate of the I^+S_z term would be enhanced by any one of these mechanisms. However, if $^3J_{HH}=10$ Hz, and if $\tau=1$ ms, the amplitude of the antiphase terms that can build up in an interval τ is limited to $\sin(\pi^3J_{HH}\tau)=0.03$. The fact that the echoes are not modulated indicates that the buildup of the antiphase terms is not cumulative in the course of the multiple-pulse train. Contributions of antiphase terms to the average relaxation rates are therefore negligible in multiple refocusing experiments. In effect, we therefore detect the transverse relaxation rates of in-phase components $R_2^{app}(I_x)$ which are not significantly "contaminated" by R_2^{app} $(2I_yS_z)$. The use of different τ values may however lead to small variations of R_2^{app} (see Tables 1–3). In experiments using a single refocusing pulse, the scalar-coupling interaction cannot be quenched, so that the decay rate is determined by the average of in-phase and antiphase relaxation rates. The scalar-coupling interaction evolves on a timescale that is faster than the relaxation processes and averages the two relaxation rate constants. Typical $^3J_{HH}$ couplings are in the range of 5–10 Hz and have periods of 200 to 100 ms, which are comparable to the transverse relaxation times of 200 to 300 ms we observed. For homonuclear spin pairs with large scalar couplings (e.g., $^1J_{CC}=35$–55 Hz), contributions of antiphase terms may play a larger role even in multiple refocusing experiments.

Table 1. Apparent relaxation rates R_2^{app} of CH_3 and amide protons in CsA determined by single and multiple refocusing experiments, with direct detection of the proton signals (i.e., without transfer to ^{13}C). In all hybrid experiments, the rf amplitude was $\omega_1/(2\pi)=5.6$ kHz, so that the ratio $\gamma=\Omega_S/\omega_1$ depends on the offset of the coupling partner. In the column "Best delays τ for quenching modulations", asterisks indicate that the rf amplitude was $\omega_1/(2\pi)=4$ kHz while for the others $\omega_1/(2\pi)=5.6$ kHz. In the column "R_2^{app}(B) from multiple refocusing", the symbols in parentheses stand for (c)=circles, (s)=squares, (t)=triangles, (d)=dots. These can be identified with the corresponding symbols in Figures 3 and 6. In the hybrid experiments the τ delay was varied from 250 to 950 μs in steps of 0.5 μs.

Label in Figure 2 (ppm)	Residue and proton type	Couplings to neighbors	Main ^3J [Hz]	Offset of main coupling partner [Hz]	Ratio $\gamma=(\Omega_S)/\omega_1$ in the hybrid sequence	Delays τ [μs] where echo modulations are worst in hybrid	Best delays τ [μs] for quenching modulations (ν_{rep}, Hz)	Even-numbered echoes 2*n* observed for CPMG	R_2^{app}(B) [s^{-1}] from multiple refocusing (CPMG)	R_2^{app}(A) [s^{-1}] from single refocusing	R_1 [s^{-1}]
a (1.08)	Val5 CH^{γ}_3	$^3J(H^{\gamma}H^{\beta})$ $^4J(H^{\gamma}H^{\gamma})$ $^4J(H^{\gamma}H^{\alpha})$	6.55	710	0.13	705	400 (1125) 550 (816)* 875 (533)*	1,10,…250 1,10,…200 1,6,…120	3.61(c)±0.08 3.62(s)±0.08 3.78(t)±0.12	4.34±0.14	2.15
b (1.27)	D-Ala8 CH^{β}_3	$3J(H^{\beta}H^{\alpha})$ $4J(H^{\beta}H^{N})$	6.75	1774	0.32	258 520 819	320 (1371) 350 (1267) 590 (788) 690 (680)	1,12,…300 1,12,…300 1,8,…160 1,8,…160	3.28(s)±0.04 3.27(t)±0.04 3.31(d)±0.05 3.19±0.09	6.39±1.22	2.36
c (1.37)	Ala7 CH^{β}_3	$3J(H^{\beta}H^{\alpha})$ $4J(H^{\beta}H^{N})$	7.2	1581	0.28	295 600 927	430 (1054) 680 (690) 710 (663) 780 (593)*	1,10,…200 1,8,…120 1,8,…120 1,6,…120	3.58(c)±0.03 3.77(s)±0.04 3.76(t)±0.07 3.69±0.09	6.81±1.22	2.53
o (7.18)	D-Ala8 H^N	$^3J(H^NH^{\alpha})$ $^4J(H^NH^{\beta})$ $^4J(H^NH^{\alpha}$ $i+1)$	8	1170	0.21	407 737	534.75 (863) 584.75 (794)	1,8,…200 1,8,.144	5.40(t)±0.10 5.65(d)±0.15	6.56±0.31	1.87
p (7.48)	Val5 H^N	$^3J(H^NH^{\alpha})$ $^4J(H^NH^{\beta})$ $^5J(H^NH^{\gamma})$ $^4J(H^NH^{\alpha}$ $i+1)$	8.4	1409	0.25	617 334	436 (1040) 486 (942) 800 (592) 850 (559)	1,10,.250 1,8,.160 1,6,…102 1,8,.112	5.56(c)±0.13 5.33(s)±0.32 5.67(t)±0.14 5.94(d)±0.28	6.36±0.3	2.15
q (7.68)	Ala7 H^N	$^3J(H^NH^{\alpha})$ $^4J(H^NH^{\beta})$ $^4J(H^NH^{\alpha}$ $i+1)$	7.4	1578	0.28	299 556 938	433 (1047) 473 (966) 700 (672)	1,10,.200 1,8,…200 1,8,…120	5.93(s)±0.2 6.03(t)±0.22 6.53(d)±0.06	6.66±0.17	2.72
r (7.98)	Abu2 H^N	$^3J(H^NH^{\alpha})$ $^4J(H^NH^{\beta})$ $^5J(H^NH^{\gamma})$ $^4J(H^NH^{\alpha}$ $i+1)$	9.8	1475	0.26	318 590	400 (1125) 450 (1011) 750 (629) 800 (592)	1,10…250 1,8….160 1,6….102 1,8,….112	6.63(c)±0.11 6.33(s)±0.30 6.84(t)±0.20 7.2(d)±0.27	7.28±0.35	2.62

2.4. Apparent Relaxation Rates R_2^{app} Expressed in Terms of Spectral Densities

We consider a three-spin subsystem with parameters that are representative for those of MeVal11 in CsA, that is, $H^{\alpha}(I)$, $H^{\beta}(S)$, and $H^{\gamma}(R)$, where the latter stands for one of the six methyl protons. The average distances between the three protons are assumed to be $<r_{IS}>=1.97$, $<r_{SR}>=1.97$, and $<r_{IR}>=3.94$ Å. In experiments with a single refocusing pulse, the initial in-phase coherence I_x will be partly converted into antiphase coherence $2I_yS_z$ through the effect of $J_{IS}={}^3J_{H\alpha H\beta}=10.9$ Hz in MeVal11 in CsA. Ignoring the long-range *I*–*R* dipolar interaction, the relaxation rate of I_x is [Eq. (2)]:[15]

$$R_2(I_x)=(d_{IS}/8)[4J_{IS}(0)+J_{IS}(\omega_I-\omega_S)+3J_{IS}(\omega_I)+6J_{IS}(\omega_S)+6J_{IS}(\omega_I+\omega_S)] \quad (2)$$

where $d_{IS}=(\mu_0/4\pi)^2(h/2\pi)^2\gamma_I^2\gamma_S^2r_{IS}^{-6}$ and $J_{IS}(\omega)=(2/5)[\tau_c/(1+\omega^2\tau_c^2)]$ is the spectral density associated with the fluctuations of the *I*–*S* dipolar interaction. If we consider the dipolar *I*–*S* and *S*–*R* interactions in the *I*–*S*–*R* system, the relaxation rate is [Eq. (3)]:

$$R_2(2I_yS_z)=(d_{IS}/8)[4J_{IS}(0)+J_{IS}(\omega_I-\omega_S)+3J_{IS}(\omega_I)+6J_{IS}(\omega_I+\omega_S)]+(d_{SR}/8)[2J_{SR}(\omega_S-\omega_R)+6J_{SR}(\omega_S)+12J_{SR}(\omega_S+\omega_R)] \quad (3)$$

where $d_{SR}=(\mu_0/4\pi)^2(h/2\pi)^2\gamma_S^2\gamma_R^2r_{SR}^{-6}$. For a homonuclear proton *I*–*R*–*S* system, we may assume that $J_{IS}(\omega_I-\omega_S)=J_{IS}(0)$, $J_{SR}(\omega_S-\omega_R)=J_{SR}(0)$, $J_{IS}(\omega_I+\omega_S)=J_{IS}(2\omega)$, $J_{SR}(\omega_S+\omega_R)=J_{SR}(2\omega)$, $J_{IS}(\omega)=J_{SR}(\omega)$, and $J_{IS}(\omega)=J_{SR}(\omega)=J(\omega)$, hence [Eq. (4)]:

$$R_2(2I_yS_z)-R_2(I_x)=-(d_{IS}/8)[6J_{IS}(\omega)]+(d_{SR}/8)[2J_{SR}(0)+6J_{SR}(\omega)+12J_{SR}(2\omega)] \quad (4)$$

If $d_{IS}=d_{SR}$ then $R_2(2I_yS_z)-R_2(I_x)=(d_{SR}/8)[2J_{SR}(0)+12J_{SR}(2\omega)]$. Since the difference depends on both $J(0)$ and $J(2\omega)$, the

Table 2. Apparent relaxation rates R_2^{app} of all backbone H^{α} protons in CsA determined by single and multiple refocusing experiments, with direct detection of the proton signals, that is, without transfer to ^{13}C for indirect detection. In the column "Best delays τ for quenching modulations", asterisks indicate that the rf amplitude was $\omega_1/(2\pi)=4$ kHz while for the others $\omega_1/(2\pi)=5.6$ kHz. In the column for "R_2^{app}(B) from multiple refocusing", the symbols in brackets stand for (c) = circles, (s) = squares, (t) = triangles, (d) = dots. These can be identified with the corresponding symbols in Figures 4 and 7. In the hybrid experiments the τ delay was varied from 250 to 950 μs in steps of 0.5 μs.

Label in Figure 2 (ppm)	Residue and proton type	Couplings to neighbors	Main ^3J [Hz]	Offset of main coupling partner [Hz]	Ratio $\gamma=(\Omega_S)/\omega_1$ in the hybrid sequence (rf amplitude, kHz)	Delays τ [μs] where echo modulations are worst in hybrid	Best delays τ [μs] for quenching modulations (ν_{rep}, Hz)	Even-numbered echoes $2n$ observed for CPMG	R_2^{app}(B) [s^{-1}] from multiple refocusing (CPMG)	R_2^{app}(A) [s^{-1}] from single refocusing	R_1 [s^{-1}]
d (4.53)	Ala7 CH^{α}	$^3J(H^{\alpha}H^{\beta})$ $^3J(H^{\alpha}H^{N})$ $^4J(H^{\alpha}H^{N}$ $i+1)$	7.2 7.4	1581 1576	0.28 (5.6) 0.28 (5.6)	295 556 929	700 (672) 750 (629) 800 (592)	1,6,…180 1,6,…180 1,6,…180	1.23(c) ± 0.03 1.24(s) ± 0.02 1.22(t) ± 0.03	6.75 ± 1.40	0.95
e (4.67)	Val5 CH^{α}	$^3J(H^{\alpha}H^{\beta})$ $^3J(H^{\alpha}H^{N})$ $^5J(H^{\alpha}H^{NCH3})$ $^4J(H^{\alpha}H^{\gamma})$	8.4 8.4	1121 1408	0.20 (5.6) 0.25 (5.6)	333 620 431	510 (902) 550 (816)*	1,6,…180 1,10,…200	2.28(d) ± 0.06 2.06(c) ± 0.08	N/A N/A	1.42
f (4.74)	Sar3 CH^{α}	$^2J(H^{\alpha}H^{\alpha})$	14	770	0.19 (4)	625	800 (580)* 850 (548)*	1,6,…120 1,6,…144	3.71(c) ± 0.36 3.74(d) ± 0.33	4.73 ± 0.87	2.89
g (4.84)	D-Ala8 CH^{α}	$^3J(H^{\alpha}H^{\beta})$ $^3J(H^{\alpha}H^{N})$ $^5J(H^{\alpha}H^{NCH3})$	8 6.75	1170 1785	0.21 (5.6) 0.32 (5.6)	258 494 819 405 738	580 (801) 650 (702)* 925 (506)*	1,6,…180 1,8,…144 1,6,…120	1.75(s) ± 0.11 1.71(c) ± 0.08 1.75(d) ± 0.11	N/A N/A	1.31
h (4.99)	MeLeu6 CH^{α}	$^3J(H^{\alpha}H^{\beta})$ $^3J(H^{\alpha}H^{\beta})$ $^5J(H^{\alpha}H^{\delta})$ $^4J(H^{\alpha}H^{\gamma})$ ^4J, $^5J(H^{\alpha}H^{NCH3})$	9.9 6	1450 1805	0.25 (4)	257 320 490 600 810	400 (1124) 730 (645)	1,12,…240 1,6,…144	2.87(s) ± 0.05 3.03(c) ± 0.07	N/A	2.36
i (5.04)	Abu2 CH^{α}	$^3J(H^{\alpha}H^{\beta})$ $^3J(H^{\alpha}H^{N})$	9.3	1680	0.42 (4)	270 307 600 875	400 (1081)* 750 (615)*	1,10,…250 1,8,…144	1.85(c) ± 0.03 1.72(s) ± 0.04	N/A	1.42
j (5.08)	MeLeu10 CH^{α}	$^3J(H^{\alpha}H^{\beta})$ $^3J(H^{\alpha}H^{\beta})$ $^5J(H^{\alpha}H^{\delta})$ $^4J(H^{\alpha}H^{\gamma})$ ^4J , $^5J(H^{\alpha}H^{NCH3})$	7	1495 1910	0.26 (4) 0.34 (4)	305 385 470 600 750	430 (1053) 840 (565)	1,12,…240 1,6,…144	4.27(c) ± 0.04 4.25(s) ± 0.1	10.78 ± 1.50	3.02
k (5.15)	MeVal11 CH^{α}	$^3J(H^{\alpha}H^{\beta})$ $^4J(H^{\alpha}H^{\gamma})$ ^4J , $^5J(H^{\alpha}H^{NCH3})$	10.9	1500	0.27 (5.6)	314 588 918	750 (629) 500 (889)* 825 (563)*	1,8,…144 1,10,…200 1,6,…120	2.07(c) ± 0.07 2.04(s) ± 0.08 1.94(t) ± 0.07	3.93 ± 0.20	1.54
l (5.35)	MeLeu4 CH^{α}	$^3J(H^{\alpha}H^{\beta})$ $^3J(H^{\alpha}H^{\beta})$ $^5J(H^{\alpha}H^{\delta})$ $^4J(H^{\alpha}H^{\gamma})$ ^4J , $^5J(H^{\alpha}H^{NCH3})$	complex multiplet	1470 1675	0.26 (4) 0.30 (4)	250 325 475 788	380 (1177) 705 (667)	1,12,…240 1,8,…160	1.52(c) ± 0.03 1.74(s) ± 0.05	N/A	1.20
m (5.47)	MeBmt1 CH^{α}	$^3J(H^{\alpha}H^{\beta})$ $^5J(H^{\alpha}H^{NCH3})$ $^4J(H^{\alpha}H^{\gamma})$	5.5	835	0.21 (4)	575	700 (655)* 800 (579)*	1,6,…144 1,6,…144	3.38(c) ± 0.05 3.60(s) ± 0.08	7.66 ± 0.43	2.15
n (5.72)	MeLeu-9 CHα	$^3J(H^{\alpha}H^{\beta})$ $^3J(H^{\alpha}H^{\beta})$ $^5J(H^{\alpha}H^{\delta})$ $^4J(H^{\alpha}H^{\gamma})$ ^4J , $^5J(H^{\alpha}H^{NCH3})$	11 4.1	1774 2235	0.32(5.6) 0.40(5.6)	258 494 818 397 650	600 (776) 690 (681) 720 (654)	1,10,..160 1,8,…152 1,8,..152	4.67(t) ± 0.1 4.35(d) ± 0.1 4.37(x) ± 0.05	N/A N/A N/A	3.08

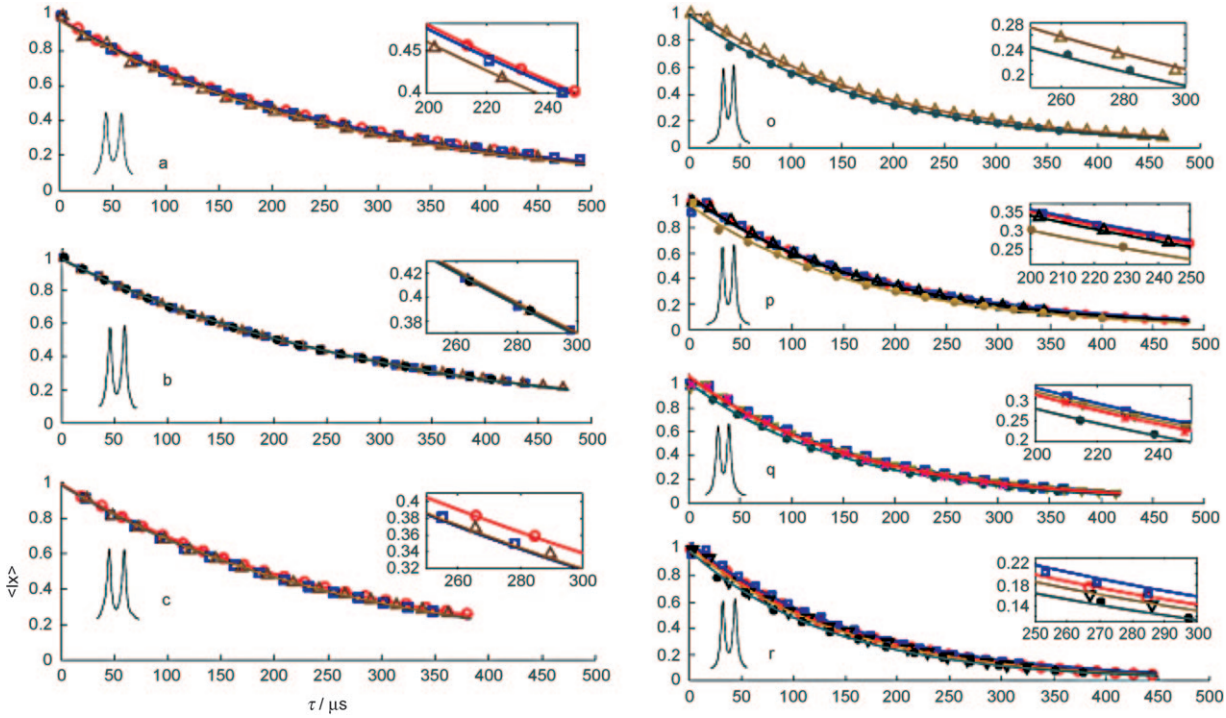

Figure 6. Monoexponential fits to the unmodulated decays of echoes recorded by stepping the number of CPMG cycles n with favorable τ intervals (see Table 1). The horizontal axis indicates the total duration $T = n(4\tau + 2\tau_\pi)$. "a" = Val5 CH^{γ}_3, "b" = D-Ala8 CH^{β}_3, "c" = Ala7 CH^{β}_3, "o" = D-Ala8 H^N, "p" = Val5 H^N, "q" = Ala7 H^N, and "r" = Abu2 H^N. The rf amplitudes, τ intervals, number of cycles n, and fitted R_2^{app} are given in Table 1.

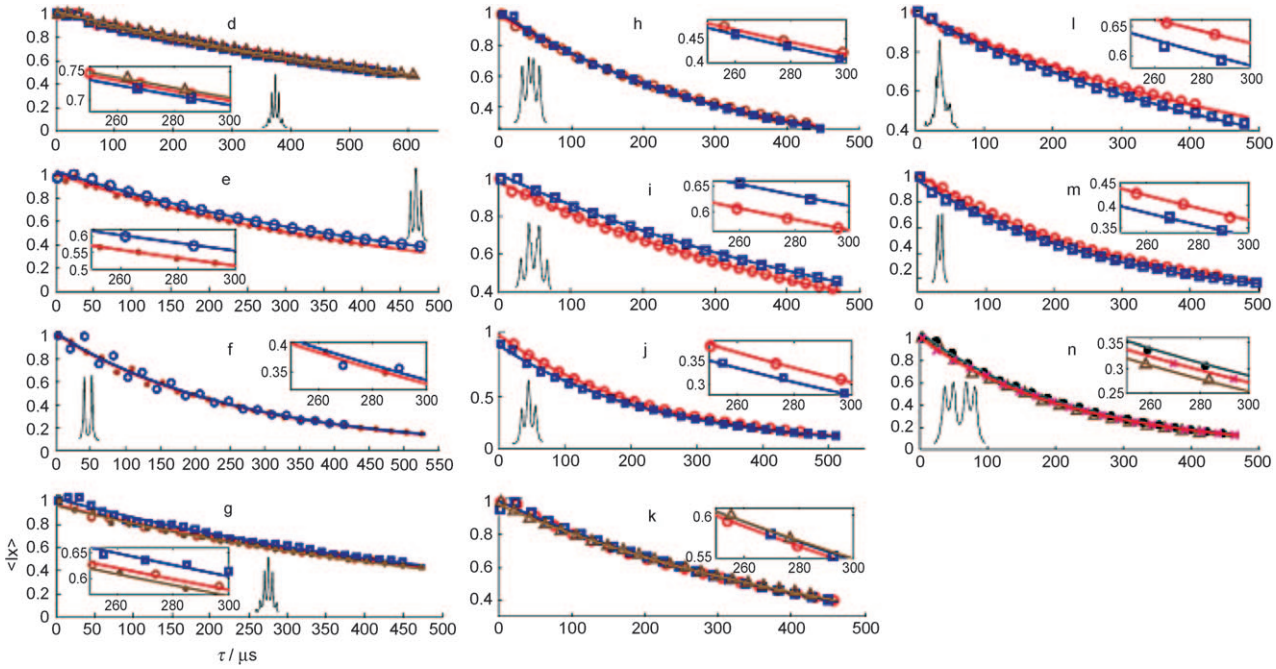

Figure 7. Monoexponential fits to the unmodulated echo decays recorded as a function of the number of cycles n for favorable τ intervals (Table 2) for H^{α} protons of the following residues: "d" = Ala7, "e" = Val5, "f" = Sar3, "g" = D-Ala8, "h" = MeLeu6, "i" = Abu2, "j" = MeLeu10, "k" = MeVal11, "l" = MeLeu4, "m" = MeBmt1, and "n" = MeLeu9. The rf amplitudes, τ intervals, number of cycles n, and fitted R_2^{app} are given in Table 2.

decay of the antiphase term $2I_yS_z$ will always be faster than the decay of I_x, irrespective of the correlation time, that is, for both slow and rapid tumbling.

For $B_0 = 11.7$ T (500 MHz for protons) and $\tau_c = 0.5$ ns, typical for medium-sized molecules such as CsA, we have a broad distribution of spectral densities $J(0) = 0.2 \times 10^{-9}$ s, $J(\omega_I) = 0.188 \times 10^{-9}$ s and $J(2\omega_I) = 0.16 \times 10^{-9}$ s, hence $R_2(I_x) = 4.42\ s^{-1}$,

Table 3. Apparent relaxation rates R_2^{app}(B) of a few protons in CsA determined by multiple refocusing, with and without transfer to ^{13}C using INEPT for indirect detection. In the last column, the symbols in brackets stand for (c) = circles, (s) = squares, (t) = triangles, (d) = dots. These can be identified with the corresponding symbols in Figures 9, 10, and 11. Asterisks indicate direct observation of proton signals. The remaining rates were obtained after transferring the proton magnetization to ^{13}C by INEPT. In the hybrid experiments the τ delay was varied from 300 to 900 μs in steps of 1 μs.

Label in Figure 2 (ppm)	Residue and proton type	Couplings to neighbors	Main ^3J [Hz]	Offset of main coupling partner [Hz]	Ratio $\gamma = (\Omega_s)/\omega_1$ in the hybrid sequence (rf amplitude, kHz)	Delays τ [μs] where echo modulations are worst in hybrid	Best delays τ [μs] for quenching modulations (ν_{rep}, Hz) (rf amplitude, kHz)	Even numbered echoes $2n$ observed for CPMG	R_2^{app}(B) [s^{-1}] from multiple refocusing (CPMG)
j (5.08)	MeLeu10	$^3J(H^\alpha H^\beta)$	7	1495	0.37 (4)	305	430 (1015) (4)	1,8,…144	8.27(d) ± 0.28
(^{13}C	CH^α	$^3J(H^\alpha H^\beta)$		1910	0.47 (4)	385	840 (554) (4)	1,6,…120	8.08(t) ± 0.40
56.49)		$^5J(H^\alpha H^\delta)$			0.37 (4)	470	430 (1053) (5.6)*	1,12,…240	4.27(s)*
		$^4J(H^\alpha H^\gamma)$			0.47 (4)	600	840 (565) (5.6)*	1,6,…144	4.25(c)*
		^4J,				750			
		$^5J(H^\alpha H^{NCH3})$							
k (5.15)	MeVal11	$^3J(H^\alpha H^\beta)$	10.9	1500	0.16 (9)	314	400 (1132) (6)	1,10,…220	5.91(d) ± 0.14
(^{13}C	CH^α	$^4J(H^\alpha H^\gamma)$			0.16 (9)	588	800 (594) (6)	1,10,…160	5.26(t) ± 0.17
57.18)		^4J ,			0.16 (9)	918	400 (1132) (6)*	1,10,…220	2.2(s)*
		$^5J(H^\alpha H^{NCH3})$			0.16 (9)		800 (594) (6)*	1,10,…160	1.99(c)*
n (5.72)	MeLeu9	$^3J(H^\alpha H^\beta)$	11	1774	0.44 (4)	258	690 (664) (4)	1,6,…120	7.96(t) ± 0.3
(^{13}C	CH^α	$^3J(H^\alpha H^\beta)$	4.1	2235	0.55 (4)	494	720 (654) (4)	1,6,…120	8.01(d) ± 0.28
47.15)		$^5J(H^\alpha H^\delta)$			0.32 (4)	818	690 (681) (5.6)*	1,8,…152	4.35(c)*
		$^4J(H^\alpha H^\gamma)$			0.40 (4)	397	720 (654) (5.6)*	1,8,…152	4.37(s)*
		^4J ,				650			
		$^5J(H^\alpha H^{NCH3})$							
s (0.87)	Abu2	$^3J(H^\gamma H^\beta)$	N/A	400	0.10 (4)	N/A	500 (444) (4)	1,10,…160	2.42(d) ± 0.17
(^{13}C	$CH^\gamma{}_3$	$^3J(H^\gamma H^\beta)$					800 (289) (4)	1,10,…120	2.73(t) ± 0.24
9.88)		$^4J(H^\gamma H^\alpha)$							
t (0.73)	MeBmt1	$^3J(H^\delta H^\gamma)$	N/A	450	0.11 (4)	N/A	500 (444) (4)	1,10,…160	3.68(d) ± 0.20
(^{13}C	CH^δ	$^4J(H^\delta H^\beta)$					750 (307) (4)	1,10,…120	3.85(t) ± 0.33
16.79)		^4J							
		^4J							

$R_2(2I_yS_z) = 7.24$ s^{-1}, so that $R_2(2I_yS_z) - R_2(I_x) = 2.82$ s^{-1} . If the third spin is ignored in the calculations, we have $R_2(2I_yS_z) - R_2(I_x) = 1.36$ s^{-1}. In peptides and proteins, the antiphase terms will relax faster. However, for an isolated pair the in-phase term will relax faster. All protons *R* that are within a radius of about 5 Å from spin *S* will increase the difference $R_2(2I_yS_z) - R_2(I_x)$.

In experiments with a single refocusing pulse, the buildup and relaxation of the antiphase term $2I_yS_z$ explains why the echo decays are faster. The rate measured by single refocusing experiments (Carr and Purcell's Method "A") is determined by [Eq. (5)]:

$$R_2^{app}(A) = 1/2\,[R_2(2I_yS_z) + R_2(I_x)] \tag{5}$$

while the rate measured by multiple refocusing experiments (Carr and Purcell's Method "B") corresponds to [Eq. (6)]:

$$R_2^{app}(B) = R_2(I_x) \tag{6}$$

The difference [Eq. (7)]:

$$\Delta R_2^{app} = R_2^{app}(A) - R_2^{app}(B) \tag{7}$$

depends on the number of neighboring spins and on the number of antiphase terms, that is, $2I_yS_z$, $4I_yS_zS_z'$, $8I_yS_zS_z'S_z''$ in systems of increasing complexity.

In Ala7 in CsA, H^α (labeled "d" in Figure 2B) has three ^3J couplings to the CH_3 methyl protons (*S*) and one ^3J coupling to H^N (*R*). The rates determined with a single refocusing pulse or with a train of refocusing pulses are therefore dramatically different: $R_2^{app}(A) = 6.75$ and $R_2^{app}(B) = 1.23$ s^{-1}, respectively. Many antiphase terms can appear due to the evolution under scalar couplings, including terms of the form $16I_xS_zS_z'S_z''R_z$. In such cases the difference ΔR_2^{app} can be significant.

In MeVal11, in which H^α ("*k*") has only one coupling $^3J(H^\alpha, H^\beta) = 10.9$ Hz, we observed $R_2^{app}(A) = 3.93$ and $R_2^{app}(B) = 1.94$ s^{-1} (Table 4). Note that H^β is close to two methyl groups, so that the difference of Equation (7) is large. In alanine residues, there

Table 4. R_2^{app} rates for H^α protons in MeBmt1 (resonance "*m*"), MeVal11 ("*k*"), and Sar3 ("*f*"), all of which have only one $^3J(H^\alpha, H^\beta)$ coupling.

	("*m*")	("*k*")	("*f*")
^3J (H^α, H^β) [Hz]	5.5	10.9	14
R_2^{app}(B) (multiple refocusing) [s^{-1}]	3.6	1.94	3.71
R_2^{app}(A) (single refocusing) [s^{-1}]	7.66	3.93	4.73
$\Delta R_2^{app} = R_2^{app}(A) - R_2^{app}(B)$ [s^{-1}]	4.06	1.99	1.02

are three equivalent CH^{β}_3 protons (S) coupled to H^{α} (I) and thus three terms I_yS_z, I_yS_z', and I_yS_z'' which can lead to high R_2^{app}(A) rates determined by single refocusing. For example, the decay rates of CH^{β}_3 groups determined by single refocusing experiments are $R_2^{app}(A) = 6.4\ s^{-1}$ in D-Ala8 and $R_2^{app}(A) = 6.8\ s^{-1}$ in Ala7, while multiple refocusing experiments gave $R_2^{app}(B) = 3.3$ and $3.6\ s^{-1}$ in D-Ala8 and Ala7, respectively.

From "*m*" to "*f*", the difference ΔR_2^{app} decreases. This is consistent with the less crowded environment from "*m*" to "*f*". The small difference ΔR_2^{app} of Sar3 (resonance "*f*") is due to the lack of side-chain protons that can have dipolar interactions with spin S and thus accelerate the relaxation of $2I_yS_z$. Thus, the number of neighboring spins is crucial. In single refocusing experiments, fitting of modulated decays becomes increasingly difficult with an increasing number of coupling partners with different coupling constants. (The decay rates R_2^{app}(A) obtained with single refocusing of many H^{α} protons have not been reported for this reason.)

2.5. Decay Rates R_2^{app} Determined by Indirect Detection via ^{13}C

Methyl resonances of peptide side chains often overlap in one-dimensional proton spectra, as can be seen in Figure 2B, thus preventing the integration of their peak amplitudes. For such overlapping proton resonances, the ^1H magnetization can be transferred to neighboring ^{13}C spins (which are usually resolved in ^{13}C spectra) by a sequence for INEPT applied at the top of the 2*n*th echo. Figure 8 shows a pulse sequence that

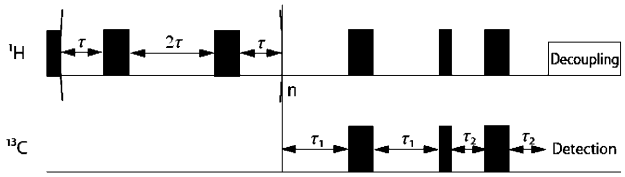

Figure 8. Pulse sequence that combines a CPMG spin-echo sequence with multiple refocusing pulses (Method "B") applied to protons with refocused INEPT. Narrow and wide rectangles represent 90° and 180° pulses, respectively. To identify suitable conditions (i.e., to avoid recoupling effects), the delay τ is varied while n is kept constant ("hybrid" experiments). To measure the rates R_2^{app}(B), τ is kept constant and n is stepped. Matched delays $\tau_1 = 1/(4^1J_{CH})$ and $\tau_2 = 1/(6^1J_{CH})$ where used to achieve efficient transfer for both CH and CH_3 systems.

combines multiple or single refocusing of protons with refocused INEPT. The signal is observed on ^{13}C but its intensity is proportional to the proton magnetization at the top of the 2*n*th echo. Differences between directly measured rates $R_2^{app}(^1H–^{12}C)$ of the protons attached to ^{12}C and indirectly measured rates $R_2^{app}(^1H–^{13}C)$ of protons attached to ^{13}C give insight into the contribution of the $^{13}C–^1H$ dipolar coupling. Of course, a comparison is only possible when the signals of the ^1H attached to ^{12}C can be resolved in the proton spectrum, without transfer by INEPT.

The blue curve in Figure 9A shows ^{13}C signals, observed after the transfer from $^1H^{\alpha}$ to $^{13}C^{\alpha}$ in MeVal11 at the top of the

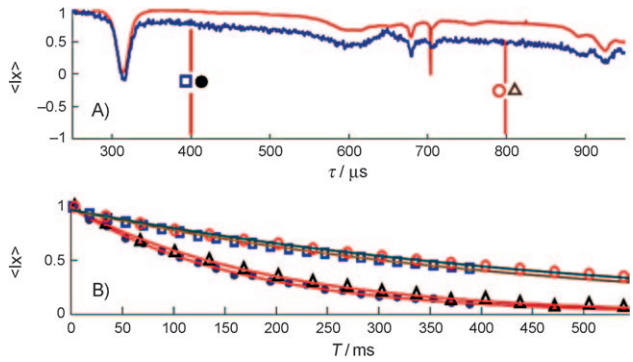

Figure 9. A) The blue curve displays the amplitude of the 120th echo ($n = 60$) of the H^{α} proton "*k*" as a function of τ, observed indirectly by transferring the magnetization of $^1H^{\alpha}$ to $^{13}C^{\alpha}$ by INEPT at the end of the echo train (see pulse sequence of Figure 8). The red curve shows the amplitude of the same H^{α} proton "*k*", again at the top of 120th echo ($n = 60$), by direct observation of the H^{α} proton signal. Since the sample was not isotopically enriched, most H^{α} protons have ^{12}C nuclei as neighbors. The proton rf carrier was positioned at 5.15 ppm to be on-resonance for H^{α}, while the ^{13}C rf carrier was set at 57.18 ppm. The rf amplitude of the proton refocusing pulses was $\omega_1/(2\pi) = 9.0$ kHz (pulse length $\tau_\pi = 27.8$ µs) and the offset of the coupling partner H^{β} was $\Omega_S/(2\pi) = 1.5$ kHz, hence the tilt parameter was $\Omega_S/\omega_1 = 0.16$. Favorable intervals $\tau = 400$ µs (squares and dots) and 800 µs (circles and triangles) were chosen to avoid echo modulations. B) Experimental decays recorded with and without ^{13}C detection for increasing n, using τ intervals 400 or 800 µs. Dots and triangles correspond to decays of H^{α} attached to ^{13}C while squares and circles correspond to decays of the same H^{α} attached to ^{12}C. Dots: $\tau = 400$ µs and $n = 1, 10, 20, \ldots, 220$, so that $0 < T < 389$ ms. The fit gave $R_2^{app}(B) = 5.91\ s^{-1}$. Triangles: $\tau = 800$ µs, $0 < T < 539$ ms, which yielded $R_2^{app}(B) = 5.26\ s^{-1}$. Squares: $\tau = 400$ µs, $0 < T < 389$ ms, which gave $R_2^{app}(B) = 2.2\ s^{-1}$. Circles: $\tau = 800$ µs, $0 < T < 539$ ms, leading to $R_2^{app}(B) = 1.99\ s^{-1}$.

120th echo ($n = 60$), as a function of τ, that is, using the hybrid approach. The proton rf carrier was positioned on-resonance for H^{α} in MeVal11 at 5.15 ppm, while the rf carrier for ^{13}C was set at 57.18 ppm. Correlations between such pairs can easily be observed in heteronuclear single-quantum coherence (HSQC) experiments. The red curve in Figure 9A shows amplitudes of the same H^{α} proton in MeVal11 observed directly at the top of the 120th echo (the proton signal is well resolved in this case). Not surprisingly, the recoupling conditions (revealed by dips in the curves) precisely coincide in the two schemes. Thus the same scheme can be safely applied for overlapping proton resonances. The blue curve in Figure 9A decays faster than the red curves. To determine R_2^{app}(B) with multiple refocusing, the best delays to avoid recoupling were found to be $\tau = 400$ µs (squares and dots) and $\tau = 800$ µs (circles and triangles). Figure 9B shows monoexponential fits to the experimental decays recorded for increasing n, using intervals $\tau = 400$ and 800 µs. The decay of the ^1H attached to ^{12}C (squares and circles) is evidently slower than the decay of the ^1H attached to ^{13}C (triangles and dots). Experimental parameters and measured rates R_2^{app}(B) are given in the caption to Figure 9 and in Table 5. A few more protons attached to ^{13}C were studied with the hybrid sequence (Figure 10) and by monoexponential fitting to exponential decays (Figure 11).

Thus, the rates "*n*" > "*j*" > "*k*" of R_2^{app}(B) of protons attached to ^{13}C follow the same trends as R_2^{app}(B) and R_1 for protons at-

Table 5. Comparison of rates R_2^{app}(B) of ^{1}H attached to ^{13}C with those of ^{1}H attached to ^{12}C.

$R_2^{app}(^1H–^{13}C)$ [s^{-1}] (ν_{rep}, Hz)	$R_2^{app}(^1H–^{12}C)$ [s^{-1}] (ν_{rep}, Hz; $\Omega_S/(2\pi)$, Hz)	$R_1(^1H–^{12}C)$ [s^{-1}]
8.01 ("*n*") (654)	4.37 ("*n*") (654; 1774, 2235)	3.08 ("*n*")
8.08 ("*j*") (554)	4.25 ("*j*") (565; 1495, 1910)	3.02 ("*j*")
5.26 ("*k*") (594)	2.02 ("*k*") (594; 1500)	1.54 ("*k*")

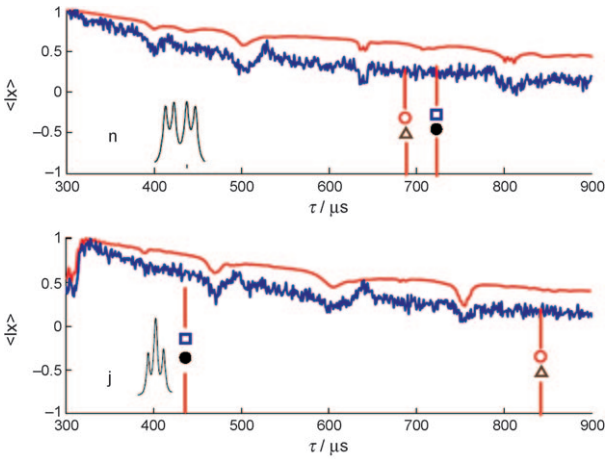

Figure 10. Blue curves: indirectly detected echo amplitudes of ^{1}H attached to ^{13}C recorded with multiple refocusing followed by INEPT as a function of τ at the top of the 200th echo ($n=100$). Resonance "*n*" corresponds to the CH$^\alpha$ residue of MeLeu9 and "*j*" to the CH$^\alpha$ residue of MeLeu10. Red curves: directly detected echo amplitudes of ^{1}H attached to ^{12}C at the top of the 200th echo without INEPT. The rf amplitudes, the offsets of the coupling partners, the chemical shifts (in ppm) of the spins that are on-resonance with the rf carrier, the types and magnitudes of the scalar couplings, the ratios $\gamma=\Omega_S/\omega_1$, and the delays τ where the echo modulations are most pronounced are summarized in Table 3.

tached to ^{12}C. The relaxation of methine protons H$^\alpha$ ("*n*", "*j*", and "*k*") is dominated by the one-bond ^{1}H–^{13}C dipolar interaction, which has a magnitude comparable to that between two geminal methylene protons.

In the slow tumbling limit, transverse relaxation is dominated by the $J(0)$ term of the spectral density, hence [Eq. (8)]:

$$R_H(^1H-^{13}C) = (d_{IC}/8)[4J_{IC}(0)] + (d_{IS}/8)[5J_{IS}(0)] \quad (8)$$

where we consider a three-spin system in which the vicinal protons I and S are coupled through $^3J_{IS}$. $J(0)$ is equal to the rotational correlation time τ_c and $d_{IC}=(\mu_0/4\pi)^2(h/2\pi)^2\gamma_I^2\gamma_C^2 r_{IC}^{-6}$ while $d_{IS}=(\mu_0/4\pi)^2(h/2\pi)^2\gamma_I^2\gamma_S^2 r_{IS}^{-6}$. If the proton is bound to ^{12}C, the relaxation rate is [Eq. (9)]:

$$R_H(^1H-^{12}C) = (d_{IS}/8)5J_{IS}(0) \quad (9)$$

If we assume $r_{IS}=1.97$ Å between two vicinal protons and $r_{IC}=1.02$ Å for a ^{13}C–^{1}H pair, we find $(5/8)\,d_{IS}=2.47\times10^9$ s^{-2} and $(4/8)\,d_{IC}=4.3\times10^9$ s^{-2}. Thus, in such a three-spin system $R_H(^1H–^{13}C)/R_H(^1H–^{12}C)=2.74$. This is confirmed experimentally for H$^\alpha$ in MeVal11 (resonance "*k*" in Figure 2B) where the ratio $R_2^{app}(^1H–^{13}C)/R_2^{app}(^1H–^{12}C)=5.26/1.99$ s$^{-1}=2.64$ (Table 3). The main source of relaxation for this H$^\alpha$ proton attached to ^{12}C is the vicinal proton. For MeLeu10 and MeLeu9 the presence of two vicinal H$^\beta$ protons coupled to H$^\alpha$ decreases the ratio $R_2^{app}(^1H–^{13}C)/R_2^{app}(^1H-^{12}C)$.

When combining a CPMG sequence with the INEPT technique, the refocusing pulses bring about an ideal inversion of the on-resonance proton I, which is therefore effectively decoupled from the directly bound ^{13}C spin C, while the off-resonance proton S' experiences a very small residual $^2J_{CH}$ heteronuclear coupling as the refocusing pulses fail to bring about an ideal inversion for this proton. However, this residual coupling does not affect the I_x coherence of the on-resonance spin.

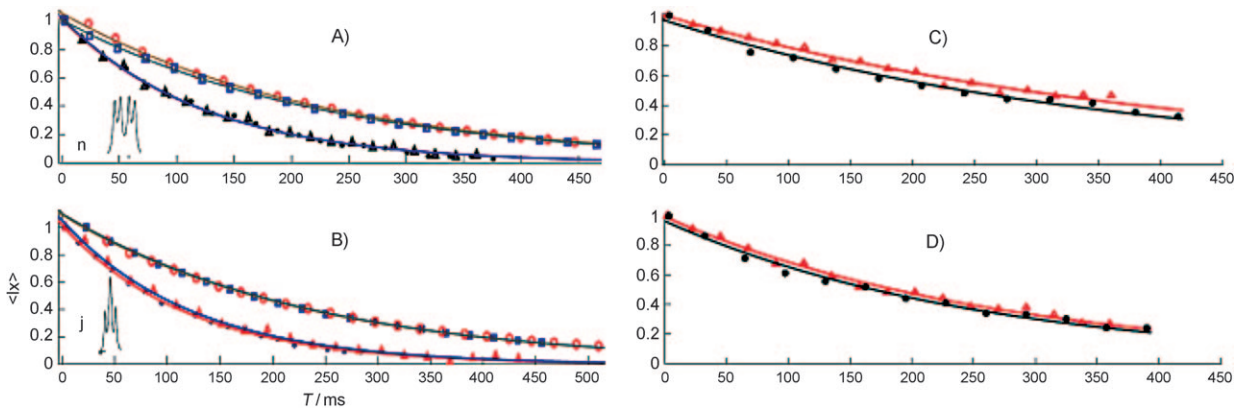

Figure 11. Monoexponential fits to unmodulated echo decays recorded as a function of the number of cycles n for favorable τ intervals (Table 3). At the end of the echo train, the proton magnetization was transferred by INEPT to ^{13}C for indirect detection. In (A) and (B), triangles and dots correspond to ^{1}H attached to ^{13}C while circles and squares represent ^{1}H attached to ^{12}C. In (C) and (D), the triangles and dots correspond to ^{1}H attached to ^{13}C. In (A), resonance "*n*" corresponds to H$^\alpha$ in MeLeu9, in (B) resonance "*j*" to H$^\alpha$ in MeLeu10, in (C) resonance "*s*" to Abu2 CH$^\gamma_3$, and in (D) resonance "*t*" to MeBmt1 CH$^\delta$. The unmodulated decays were fitted with monoexponential functions. The rf amplitudes, the offsets Ω_S of the coupling partners, the chemical shifts of the nuclei that were on-resonance (in ppm), the ratios $\gamma=\Omega_S/\omega_1$, the types and magnitudes of the scalar couplings, and the delays (τ in µs) where echo modulations are most pronounced are given in Table 3.

3. Conclusions

This study demonstrates how apparent transverse relaxation rates R_2^{app} of backbone and side-chain protons in peptides can be readily determined by quenching homonuclear scalar couplings. For backbone protons, the rates R_2^{app} and R_1 and the intensities of NOESY cross peaks are correlated with the environment. In the cyclic undecapeptide CsA, the correlation is quite robust when comparing similar protons belonging to the same amino acid residues. The rates R_2^{app} of overlapping proton resonances can be measured by combining a multiple refocusing sequence with the INEPT technique. In cases where the proton resonances are resolved, a comparison of the rates R_2^{app} of protons attached to ^{12}C with those of the same protons attached to ^{13}C allows one to determine the contribution to relaxation from ^{13}C–^{1}H dipolar couplings. Thus, the measurement of apparent proton transverse relaxation rates opens new avenues for dynamic studies.

Experimental Section

All spectra were recorded with a Bruker Avance spectrometer with a field $B_0 = 11.74$ T (500 MHz for ^{1}H) at a temperature $T = 300$ K. The sample concentration of CsA (Sigma–Aldrich) was 20 mM in $CDCl_3$.

Acknowledgements

We are indebted to Martial Rey for valuable assistance. This work was supported by the Swiss National Science Foundation (FNSNF), the Ecole Polytechnique Fédérale de Lausanne (EPFL), the Swiss Commission for Technology and Innovation (CTI), and the CNRS (France).

Keywords: multiple refocusing · NMR spectroscopy · scalar couplings · spin echoes · transverse relaxation

[1] E. L. Hahn, *Phys. Rev.* **1950**, *80*, 580–594.
[2] H. Y. Carr, E. M. Purcell, *Phys. Rev.* **1954**, *94*, 630–638.
[3] S. Meiboom, D. Gill, *Rev. Sci. Instrum.* **1958**, *29*, 688–691.
[4] R. Freeman, H. D. W. Hill in *Dynamic NMR Spectroscopy* (Eds.: L. M. Jackman, F. A. Cotton), Academic Press, New York, **1975**.
[5] E. O. Stejskal, J. E. Tanner, *J. Chem. Phys.* **1965**, *42*, 288–292.
[6] J. E. Tanner, *J. Chem. Phys.* **1970**, *52*, 2523–2526; erratum, J. E. Tanner, *J. Chem. Phys.* **1972**, *57*, 3586.
[7] C. S. Johnson, *Prog. Nucl. Magn. Reson. Spectrosc.* **1999**, *34*, 203–256.
[8] J. P. Carver, R. E. Richards, *J. Magn. Reson.* **1972**, *6*, 89–105; erratum, J. P. Carver, R. E. Richards, *J. Magn. Reson.* **1972**, *8*, 206.
[9] O. Millet, J. P. Loria, C. D. Kroenke, M. Pons, A. G. Palmer, *J. Am. Chem. Soc.* **2000**, *122*, 2867–2877.
[10] K. Kloiber, R. Konrat, *J. Biomol. NMR* **2000**, *18*, 33–42.
[11] J. Dittmer, G. Bodenhausen, *J. Am. Chem. Soc.* **2004**, *126*, 1314–1315.
[12] J. Dittmer, G. Bodenhausen, *ChemPhysChem* **2004**, *5*, 1750–1754.
[13] M. Tollinger, N. R. Skrynnikov, F. A. A. Mulder, J. D. Forman-Kay, L. E. Kay, *J. Am. Chem. Soc.* **2001**, *123*, 11341–11352.
[14] F. Massi, M. J. Grey, A. G. Palmer, *Protein Sci.* **2005**, *14*, 735–742.
[15] J. Cavanagh, W. J. Fairbrother, A. G. Palmer, M. Rance, N. J. Skelton, *Protein NMR Spectroscopy—Principles and Practice, 2nd ed.*, Academic Press, San Diego, **2007**.
[16] M. Verde, S. Ulzega, F. Ferrage, G. Bodenhausen, *J. Chem. Phys.* **2009**, *130*, 074506.
[17] S. Ulzega, M. Verde, F. Ferrage, G. Bodenhausen, *J. Chem. Phys.* **2009**, *131*, 224503.
[18] B. Baishya, T. F. Segawa, G. Bodenhausen, *J. Am. Chem. Soc.* **2009**, *131*, 17538–17539.
[19] J. Dittmer, G. Bodenhausen, *ChemPhysChem* **2006**, *7*, 831–836.
[20] Z. Tosner, A. Skoch, J. Kowalewski, *ChemPhysChem* **2010**, *11*, 638–645.
[21] N. Aeby, G. Bodenhausen, *Chem. Phys. Lett.* **2008**, *463*, 418–421.
[22] T. Meersmann, G. Bodenhausen, *J. Magn. Reson.* **1995**, *115*, 277–282.
[23] T. F. Segawa, N. Aeby, G. Bodenhausen, *Phys. Chem. Chem. Phys.* **2010**, *12*, 9772–9776.
[24] H. Kessler, H. R. Loosli, H. Oschkinat, *Helv. Chim. Acta* **1985**, *68*, 661–681.
[25] H. R. Loosli, H. Kessler, H. Oschkinat, H. P. Weber, T. J. Petcher, A. Widmer, *Helv. Chim. Acta* **1985**, *68*, 682–704.
[26] K. Gopalakrishnan, N. Aeby, G. Bodenhausen, *ChemPhysChem* **2007**, *8*, 1791–1802.

Received: April 30, 2010
Published online on October 11, 2010

